

Simultaneous measurement of HOM-like and N00N-like two-photon wavepackets in a Mach-Zehnder interferometer

Heonoh Kim, Sang Min Lee, and Han Seb Moon

Department of Physics, Pusan National University, Busan 609-735, South Korea

e-mail address: hsmoon@pusan.ac.kr

We propose and experimentally demonstrate two-photon interference effects in a Mach-Zehnder interferometer in which two different kinds of two-photon states are prepared by introducing a time delay between the two input photons. The two-photon states are simultaneously prepared in a symmetrically superposed state with two temporally separated photons in two different spatial modes or in the same spatial mode within the interferometer. We observe two-photon interference fringes involving both the Hong-Ou-Mandel interference effect and the interference of path-entangled two-photon states simultaneously in a single interferometric setup. The observed two-photon interference effect can provide a simultaneous observation of the interferometric properties of the single-photon and two-photon wavepackets.

The Hong-Ou-Mandel (HOM) interference effect [1] and the interference of the path-entangled two-photon state [2], the so-called N00N state [3], have played an important role in the fundamental study of quantum mechanics and in exploring quantum information technology [4,5]. From the late 1980s, various kinds of two-photon interference experiments have been performed to distinguish the quantum mechanical treatment of optical interference phenomena from conventional classical optics [6,7]. These experiments have shown successfully that the interference of correlated photons cannot be explained by any classical wave theory; instead, they should be viewed as interference between superposed probability amplitudes. Thereafter, a number of experiments have been performed to explicitly understand two-photon quantum interference effects such as the HOM effect and the N00N-state interference [8-14]. Recently, we have reported that the two-photon quantum interference effect was observed in the most generalized two-photon interferometric scheme even when two photons of the correlated pair state did not arrive at the same beam splitter at the same time in the fully unfolded HOM scheme as well as the N00N-state interferometer [15].

Meanwhile, two-photon interference in a Mach-Zehnder interferometer (MZI) has also been utilized as a practical tool to investigate two-photon wavepacket interference phenomena [2,12,16,17]. In particular, the most interesting feature can be shown when two correlated photons are incident on the MZI with a time delay that is considerably longer than their coherence time. Even in the case of a large time delay between two input photons, if the two-photon states are still in symmetrically superposed states to exhibit two-photon interference effects, then we can simultaneously observe the coherence properties of the single-photon and two-photon wavepackets from the measured two-photon interference fringes. There are many

literatures dealing with two-photon quantum interference experiments in a MZI. However, here we show explicit analysis for the origin of the interference phenomena which occur when spatially bunched/anti-bunched two-photon states within the MZI are involved.

In this paper, we report on the experimental demonstration of quantum interference effects with two kinds of two-photon states in a conventional MZI. The two distinct two-photon states are prepared by introducing a time delay between two incident photons at the first beam splitter of the MZI. The two photons are well separated by a time interval that is longer than the coherence time of both the individual single photons and the two-photon states. Under this condition, we introduce HOM-like and N00N-like two-photon states within the MZI to distinguish the conventional HOM and N00N states. The HOM-like state can be defined as a superposed input state with a large time delay between the two single photons in two different spatial modes. However, the entire state of the two photons is in a symmetrically superposed state in the two spatial modes. On the other hand, in the case of the N00N-like state, the two single photons with large time delay are in the same spatial mode. Experimental demonstrations employing the HOM-like state have been performed by using the polarization-entangled state [10] as well as the frequency-entangled state [18]. Recently, the two-photon quantum interference of the N00N-like state was successfully demonstrated to show that the temporal separation between two sequential photons in the same spatial mode does not degrade the phase super-resolution, as in the case of the conventional N00N state [14].

The conceptual scheme for the generation of the HOM-like and N00N-like two-photon states is depicted in Fig. 1. As is well known, the conventional two-photon N00N state can easily be generated from the HOM interference effect when two identical single photons enter BS1

simultaneously, as shown in Fig. 1(a) [2,12]. In this case, the two output photons are always probabilistically bunched up at one of the two spatial modes, which is described by the following expression,

$$|1,1\rangle_{1,2} \xrightarrow{\text{BS1}} \frac{1}{\sqrt{2}} \left(|2,0\rangle_{3,4} + e^{i2\phi} |0,2\rangle_{3,4} \right), \quad (1)$$

where the subscripts denote the two spatial modes of the input and output of BS1 and ϕ is the relative single-photon phase difference between the two arms of the MZI, which can be introduced by the path-length difference Δx_2 . On the other hand, the HOM-like and N00N-like two-photon states can be prepared by introducing a time delay $\Delta\tau_1 = \Delta x_1 / c$ between two identical photons at the input stage of the MZI. When the two photons are sufficiently separated from each other when compared with their coherence length, as shown in Fig. 1(b), the HOM bunching effect at the output ports of the BS1 does not arise anymore. In this case, the two output photons are in a superposed state that can be expressed in the following form,

$$|1(\Delta x_1), 1\rangle_{1,2} \xrightarrow{\text{BS1}} \frac{1}{\sqrt{2}} \left(|\Psi\rangle_{\text{HOM-like}} + |\Psi\rangle_{\text{N00N-like}} \right), \quad (2)$$

where,

$$\begin{aligned} |\Psi\rangle_{\text{HOM-like}} &= \frac{1}{\sqrt{2}} \left[|1\rangle_3 |1(\Delta x_1)\rangle_4 - |1(\Delta x_1)\rangle_3 |1\rangle_4 \right], \\ |\Psi\rangle_{\text{N00N-like}} &= \frac{i}{\sqrt{2}} \left[|1(\Delta x_1), 1\rangle_3 |0\rangle_4 + e^{i2\phi} |0\rangle_3 |1(\Delta x_1), 1\rangle_4 \right]. \end{aligned} \quad (3)$$

The two-photon state represented by Eq. (2) constructs a superposed state of the HOM-like and N00N-like states involving two temporally separated photons in two different spatial modes or in the same spatial mode. Then the final state at the output port of BS2 is composed of the three states,

$$|\Psi\rangle_{\text{out}} = \frac{1}{2} \left\{ \begin{aligned} &\sin \phi \left[|0\rangle_5 |1(\Delta x_1), 1\rangle_6 - |1(\Delta x_1), 1\rangle_5 |0\rangle_6 \right] \\ &-\cos \phi \left[|1(\Delta x_1)\rangle_5 |1\rangle_6 + |1\rangle_5 |1(\Delta x_1)\rangle_6 \right] \\ &+ \left[|1(\Delta x_1)\rangle_5 |1\rangle_6 - |1\rangle_5 |1(\Delta x_1)\rangle_6 \right] \end{aligned} \right\}. \quad (4)$$

Here, the first term on the right side represents a phase-sensitive N00N-like state, while the last two terms correspond to phase-insensitive HOM-like states. In the case of $\phi = 0$ and $\phi = \pi$, the output state has the form $|\Psi\rangle_{\text{out}} = |1\rangle_5 |1(\Delta x)\rangle_6$ and $|\Psi\rangle_{\text{out}} = |1(\Delta x)\rangle_5 |1\rangle_6$, respectively, which is the same form as the input state of BS1. On the other hand, when $\phi = \pi/2$, the output state has similar form as the input state of BS2.

The observation of the two-photon interference effects using the HOM-like and N00N-like states is performed at the output ports of BS2 of the MZI by

varying the path-length difference Δx_2 . It has been already known that the HOM-like state interference has a phase-insensitive effect [10,15,18], while the N00N-like state can generate a resolution-enhanced phase-sensitive fringe pattern [14]. From Eq. (4), when the two input photons are injected into BS1 with a large time delay, as shown in Fig. 1(b), the coincidence detection probability at the two output ports of the MZI is expressed as a superposition of the HOM-like peak and the N00N-like state interference fringe as follows [19],

$$P(\Delta x_2) = N_0 \left\{ 2 + V \left[f(\Delta x_2) + g(\Delta x_2) \cos \left(\frac{2\pi}{\lambda_p} \Delta x_2 \right) \right] \right\}, \quad (5)$$

where N_0 represents a constant, V is the two-photon fringe visibility, λ_p is the center wavelength of pump laser and $f(\Delta x_2)$ and $g(\Delta x_2)$ are envelope functions corresponding to the spectral properties of the detected single-photon and two-photon wavepackets, respectively.

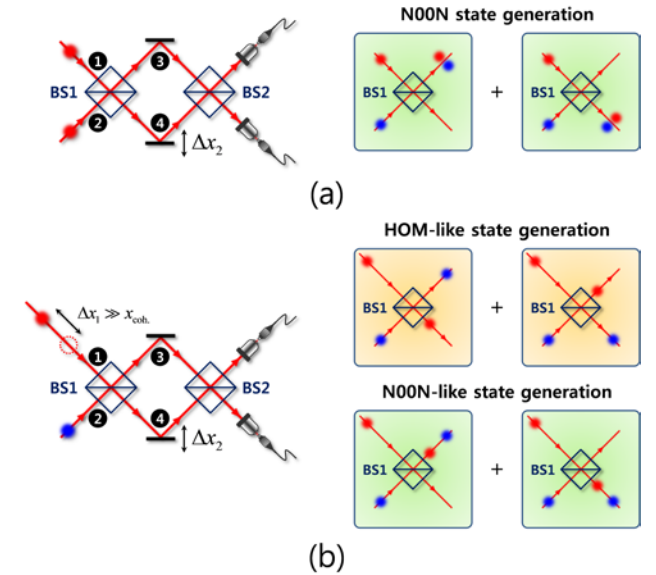


FIG. 1. Conceptual scheme for generation of (a) the conventional N00N state from the HOM interference effect at the output port of BS1 and (b) superposed state of the HOM-like and N00N-like states with large time delay between two photons at the input port of BS1.

Figure 2(a) shows the experimental setup to demonstrate the two-photon interference effects in an MZI. Correlated photon pairs at a telecommunication wavelength of 1550 nm are generated through a quasi-phase-matched spontaneous parametric down-conversion (QPM-SPDC) process in a type-0 periodically-poled lithium niobate (PPLN) crystal. We use a mode-locked picosecond fiber laser (PriTel, FFL-20-HP-PRR and SHG-AF-200) as a pumping source for QPM-SPDC, whose pulse duration is

3.5 ps at the center wavelength of 775 nm with a repetition rate of 20 MHz. In our experiments, the average pump power was set as 20 mW. With this setup, degenerate photon pairs are emitted with the full-opening angle of 4.6° in the noncollinear regime, as shown in Fig. 2(b).

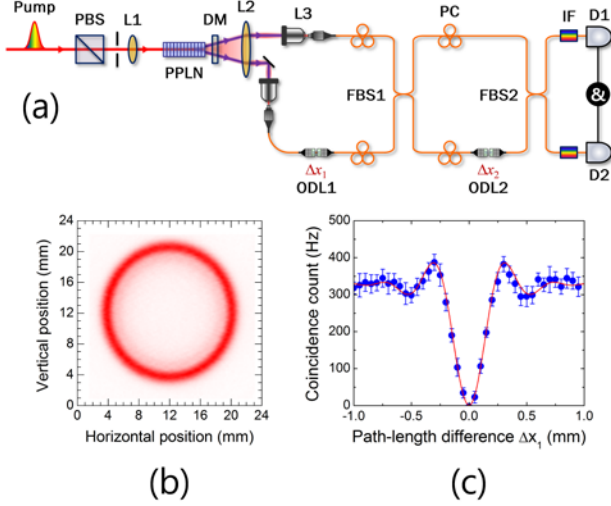


FIG. 2. (a) Experimental setup. Pump, picosecond mode-locked fiber laser (3.5 ps, 20 MHz, 775 nm, 20 mW); PBS, polarizing beam splitter; L1, L2, spherical lenses with focal length of 200 mm; PPLN, periodically-poled lithium niobate crystal (length 10 mm, grating period 19.2 μm , temperature 40°C); DM, dichroic mirror (T1550 nm/R775 nm); L3, aspherical lens with focal length of 8 mm; PC, polarization controller; ODL, optical delay line; FBS: fiber beam splitter 50/50; IF, interference filter with 6.25 nm bandwidth, D1, D2, gated-mode single-photon detection modules (Id Quantique id-210). (b) Noncollinear down-conversion image measured with single photon detector at position L2, (c) HOM dip measured at the output port of FBS1, $V = 99.74 \pm 2.03\%$.

Our experimental setup is composed of two fiber interferometers. The fiber length of each MZI arm is about 4 m. The first fiber beam splitter FBS1 acts as state manipulator and the second one, FBS2, acts as a beam combiner. Output photons from FBS2 are detected after they pass through interference filters with a bandwidth of 6.25 nm via two InGaAs/InP single-photon detection modules (Id Quantique id-210) operated in the gated mode. Electronic trigger signals are sent from the pump to the gate of the detectors by way of electric delay lines. The quantum efficiency and dead time of detectors are set as 15% and 10 μs , respectively. The coincidence resolving time window is set to be 10 ns which is very short than pulse period of 50 ns. Under these experimental conditions, the coincidence to accidental coincidence ratio was about 4.13. The pair production probability per pulse is obtained by dividing the accidental coincidence by the actual

coincidence ratio, which was estimated to be about 0.24 per pulse. Figure 2(c) shows the HOM interference fringe measured at the output port of FBS1. The fringe width is determined to be about 0.44 mm which is estimated from the rectangular-shaped interference filter with a bandwidth of 6.25 nm.

Figure 3 shows the experimental results of the two-photon interferences with the two different kinds of input states shown in Fig. 1. The conditions for the two input states before FBS2 are controlled by adjusting optical delay line ODL1 (Δx_1) before FBS1, and the two-photon coincidence fringes are measured by varying the path-length difference Δx_2 . Figure 3(a) shows the measured two-photon interference fringe arising from the conventional N00N-state input, representative of Eq. (1) when $\Delta x_1 = 0$. In the case where the input state is in a superposition of the HOM-like and N00N-like states with the introduction of a large delay, $\Delta x_1 \gg x_{\text{coh}}$, as shown in Fig. 1(b) and representative of Eq. (2), we can simultaneously observe the HOM-like and N00N-like two-photon interference fringes in Fig. 3(b). In particular, it is worth noting that the two kinds of interference effects do not affect each other. Consequently, the two detectors D1 and D2 probabilistically record the total coincidences resulting from the two kinds of interference phenomena, as expected from Eq. (4). The squared symbols represent measured coincidence counts as a function of the path-length difference Δx_2 . The gray areas in Fig 3(a) and 3(b) correspond to the phase-super-sensitive oscillatory fringe patterns with a visibility of 98%, which is estimated from Eq. (5). The solid lines denote the envelope curves, $g(\Delta x_2)$ in Eq. (5), from the Gaussian function with the full-width at half-maximum (FWHM) of 1.17 mm, which is determined by the two-photon coherence length [15]. In Fig. 3(b), the fringe width of $g(\Delta x_2)$ for simultaneous inputs of the HOM-like and N00N-like states is equal to that of the N00N state in Fig. 3(a); on the other hand, the dashed line in Fig. 3(b) represents the function of single-photon property, $f(\Delta x_2)$ in Eq. (5), which can be obtained from the interpolated plots of the phase-sensitive interference fringe, and is thus the same as the width of the single-photon wavepacket [19]. Here, the $f(\Delta x_2) = \text{sinc}(\Delta x_2 / \sigma_s)$, where σ_s is related to the single-photon bandwidth, provides a measure of the HOM-like two-photon interference fringe and is thus determined only by the interference filter used in the experiment, while the $g(\Delta x_2) = \exp[-\Delta x_2^2 / (2\sigma_T^2)]$ where σ_T is the two-photon bandwidth, determines the shape and size of the N00N-like interference fringe, which can be estimated from the pump pulse duration and the group velocity dispersion (GVD) in the pair generation process via SPDC [15]. When Δx_2 becomes $\pm \Delta x_1$ the ordinary HOM-dip

fringes are observed with a visibility of 24.5% because only one-fourth of the total two-photon amplitudes contribute to the conventional HOM interference, as shown in Figs. 3(c, d).

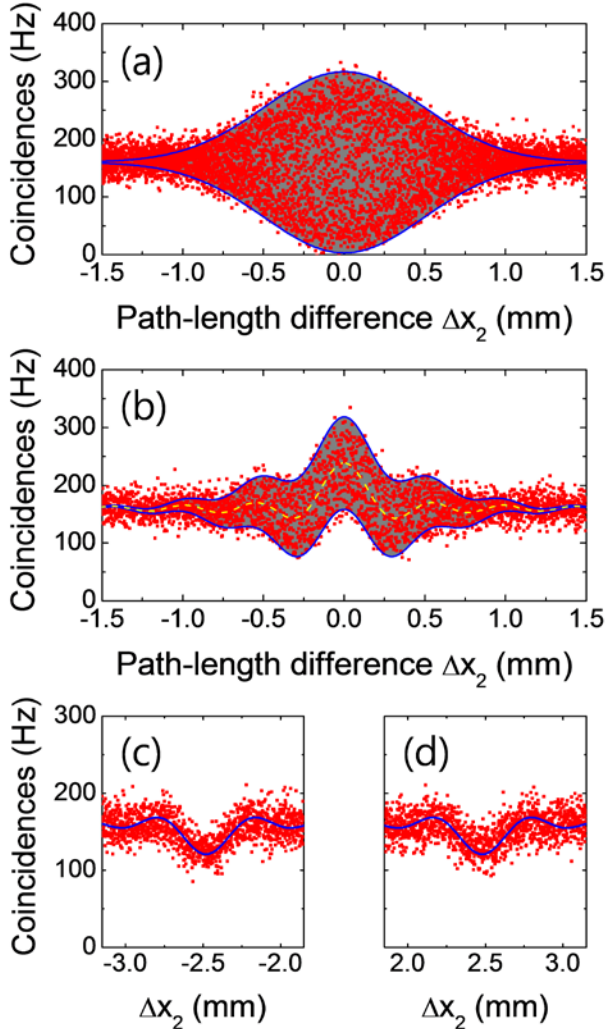


FIG. 3. Measured two-photon interference fringes for (a) conventional N00N-state input ($\Delta x_1 = 0$) and (b) simultaneous inputs of the HOM-like and N00N-like states ($\Delta x_1 = 2.5$ mm). (c) and (d) represent ordinary HOM interference dip fringes when Δx_2 becomes $\pm \Delta x_1$.

Related studies with our experiment have been reported by employing a coherently recurrent pump mode as the SPDC pump [20,21]. These papers give precise mathematical analysis of the phenomena. However, our study provide qualitative explanations both the shape of the central fringe for the case of simultaneous inputs of the HOM-like and N00N-like states, and the phase-insensitive side peak fringes arise from ordinary HOM-state inputs. In addition, the dispersion cancellation effects observed in

two-photon interference experiments involving frequency-anticorrelated photon pairs in a HOM scheme can also be explained in the context of the interference of the HOM-like state, as depicted in Fig. 1(b) [19,22]. Indeed, a large number of the two-photon quantum interference phenomena can be more expressly understood by employing superposed states such as the HOM-like and N00N-like two-photon states.

To investigate the influence of the time delay between the two input photons at FBS1 on the two-photon interference fringe pattern as shown in Fig. 3, we performed additional two experiments. Firstly, we measured interference fringes as a function of Δx_2 for various position delays Δx_1 . As shown in Fig. 4(d) and 4(e), the shape and size of the center fringe are not changed when Δx_1 is much longer than two-photon coherence length. The positions of the side dip fringes are exactly the same as the positions of $\pm \Delta x_1$ at the input port of FBS1. Secondly, we measured two-photon interference fringe as a function of Δx_1 when $\Delta x_2 = 0$. As we can see from the center positions in Fig. 4, even when the delay between the two input photons at FBS1 is longer than the single-photon coherence length ($\Delta x_1 > x_{\text{coh}}$), the two-photon interference effect originated from the HOM-like and N00N-like two-photon state simultaneously was not affected by Δx_1 because the phase-insensitive HOM-like state has no contribution to the two-photon interference effect any more as shown in Eq. (4). Therefore, the fringe visibility has a constant value of 1/3. In the special case of $\Delta x_1 = 0$, the N00N-state interference only in Fig. 3(a) is measured at the output ports of FBS2 because all of the input photons at the FBS1 can contribute to the N00N-state interference when we consider only one pair event per pulse.

In conclusion, we have demonstrated two-photon interference effects in an MZI with temporally separated two-photon states. We introduced the concept of the HOM-like and N00N-like two-photon states to distinguish the conventional two-photon state with no time delay between two photons. By introducing a large time delay in the input stage of the MZI, we prepared two kinds of symmetrically superposed states: the HOM-like and N00N-like two-photon states. The measured two-photon interference fringes involving two different kinds of input states revealed the interferometric properties of the single-photon wavepacket and the two-photon wavepacket simultaneously in a single interferometric setup. Experimental results and related analysis can clarify the origin of two-photon interference effects in a MZI more intuitively. We believe that the present results will be able to provide a more comprehensive understanding of the interference phenomena involving correlated quantum particles.

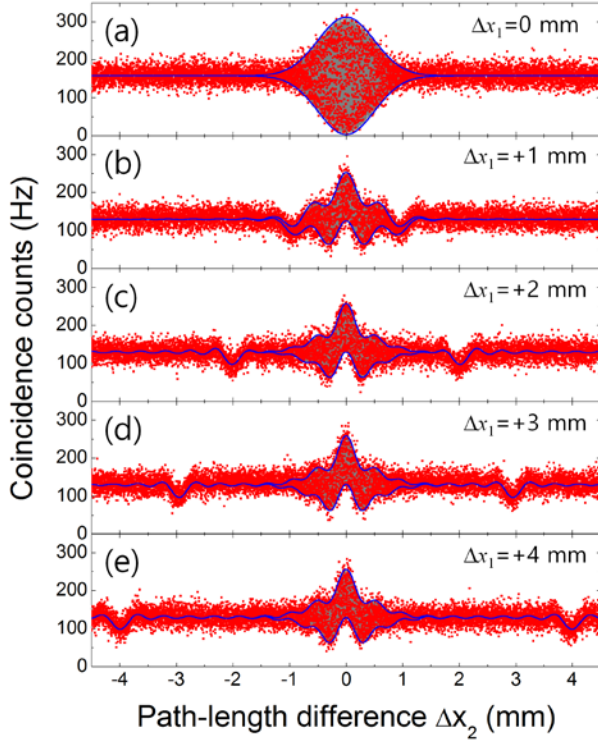


FIG. 4. Measured two-photon interference fringes as a function of Δx_2 for various delay positions Δx_1 .

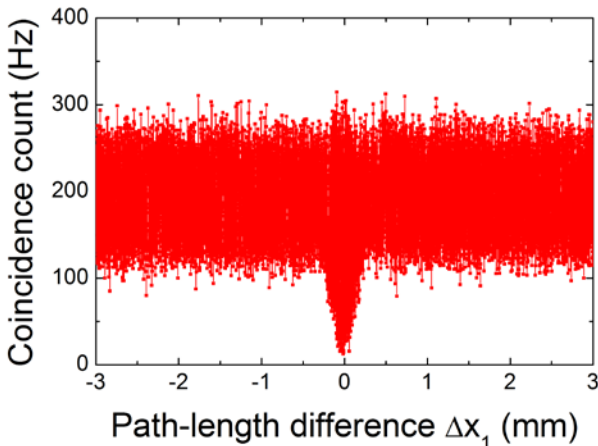


FIG. 5. Measured two-photon interference fringe as a function Δx_1 when $\Delta x_2 = 0$.

This work was supported by the National Research Foundation of Korea (NRF) grant funded by the Korea government (MSIP) (No. 2015R1A2A1A05001819, No. 2014R1A1A2055488, and No. 2014R1A1A2054719), and by the Measurement Research Center (MRC) Program for Korea Research Institute of Standards and Science.

References

- [1] C. K. Hong, Z. Y. Ou, and L. Mandel, *Phys. Rev. Lett.* **59**, 2044 (1987).
- [2] Z. Y. Ou, X. Y. Zou, L. J. Wang, and L. Mandel, *Phys. Rev. A* **42**, 2957 (1990).
- [3] H. Lee, P. Kok, and J. P. Dowling, *J. Mod. Opt.* **49**, 2325 (2002).
- [4] Z. S. Yuan, X. H. Bao, C. Y. Lu, J. Zhang, C. Z. Peng, and J. W. Pan, *Physics Reports* **497**, 1 (2010).
- [5] J. W. Pan, Z. B. Chen, C. Y. Lu, H. Weinfurter, A. Zeilinger, and M. Żukowski, *Rev. Mod. Phys.* **84**, 777 (2012).
- [6] L. Mandel, *Rev. Mod. Phys.* **71**, S274-S282 (1999).
- [7] G. Jaeger and A. V. Sergienko, Multi-photon quantum interferometry, in E. Wolf, *Progress in Optics* **42**, Elsevier Science B.V. (2001), pp. 277-324.
- [8] T. B. Pittman, D. V. Strekalov, A. Migdall, M. H. Rubin, A. V. Sergienko, and Y. H. Shih, *Phys. Rev. Lett.* **77**, 1917 (1996).
- [9] D. V. Strekalov, T. B. Pittman, and Y. H. Shih, *Phys. Rev. A* **57**, 567 (1998).
- [10] Y.-H. Kim and W. P. Grice, *J. Opt. Soc. Am. B* **22**, 493 (2005).
- [11] A. N. Boto, P. Kok, D. S. Abrams, S. L. Braunstein, C. P. Williams, and J. P. Dowling, *Phys. Rev. Lett.* **85**, 2733 (2000).
- [12] K. Edamatsu, R. Shimizu, and T. Itoh, *Phys. Rev. Lett.* **89**, 213601 (2002).
- [13] I. Afek, O. Ambar, and Y. Silberberg, *Science* **328**, 879 (2010).
- [14] X.-M. Jin, C.-Z. Peng, Y. Deng, M. Barbieri, J. Nunn, and I. A. Walmsley, *Sci. Rep.* **3**, 1779 (2013).
- [15] H. Kim, S. M. Lee and H. S. Moon, *Sci. Rep.* **5**, 9931 (2015).
- [16] J. G. Rarity, P. R. Tapster, E. Jakeman, T. Larchuk, R. A. Campos, M. C. Teich, and B. E. A. Saleh, *Phys. Rev. Lett.* **65**, 1348 (1990).
- [17] T. S. Larchuk, R. A. Campos, J. G. Rarity, P. R. Tapster, E. brakeman, B. E. A. Saleh and M. C. Teich, *Phys. Rev. Lett.* **70**, 1603 (1993).
- [18] H. Kim, H. J. Lee, S. M. Lee and H. S. Moon, *Opt. Lett.* **40**, 3061 (2015).
- [19] M. Halder, S. Tanzilli, H. de Riedmatten, A. Beveratos, H. Zbinden, and N. Gisin, *Phys. Rev. A* **71**, 042335 (2005).
- [20] O. Kwon, Y.-S. Ra, and Y.-H. Kim, *Opt. Express* **17**, 13059 (2009).
- [21] O. Kwon, Y.-S. Ra, and Y.-H. Kim, *Phys. Rev. A* **81**, 063801 (2010).
- [22] A. M. Steinberg, P. G. Kwiat, and R. Y. Chiao, *Phys. Rev. Lett.* **68**, 2421 (1992).